J. Fluid Mech. (2007), *vol.* 572, *pp.* 261–286. © 2007 Cambridge University Press
doi:10.1017/S0022112006003624 Printed in the United Kingdom

The effect of viscosity on the stability of a uniformly rotating liquid column in zero gravity

By J. P. KUBITSCHEK† AND P. D. WEIDMAN
Department of Mechanical Engineering, University of Colorado, Boulder, CO 80309-0427, USA

(Received 10 March 2006 and in revised form 11 July 2006)

An investigation of the linear temporal stability of a uniformly rotating viscous liquid column in the absence of gravity is presented. The governing parameters are the rotational Reynolds number Re and the Hocking parameter L, defined as the ratio of surface tension to centrifugal forces. Though the viscosity-independent condition $L \geqslant (k^2+n^2-1)^{-1}$ for stability to disturbances of axial wavenumber k and azimuthal mode number n has been known for some time, the preferred modes, growth rates and frequencies at onset of instability have not been reported. We compute these results over a wide range of L–Re space and determine certain asymptotic behaviours in the limits of $L \to 0$, $L \to \infty$ and $Re \to \infty$. The computations exhibit a continuous evolution toward known inviscid stability results in the large-Re limit and their ultimate transition to an $n=1$ spiral mode at small Re. While viscosity is shown to reduce growth rates for axisymmetric disturbances, it also produces a destabilizing effect for $n=2$ planar and $n=1$ spiral disturbances in certain regions of parameter space. A special feature is the appearance of a tricritical point in L–Re space at which maximum growth rates of the axisymmetric, $n=1$ spiral, and $n=2$ planar disturbances are equal.

1. Introduction

The stability of rotating liquid columns and jets is of interest for applications to liquid atomization, combustion processes, dispersion of pressure liquified gases, breakdown of vortex cores, and nozzle design for spray or coating processes, among others. This investigation addresses specifically the effect of viscosity on the stability of a uniformly rotating viscous liquid column with stress-free boundary conditions in the absence of gravity. We seek the preferred modes of instability as a function of two dimensionless parameters: L, the ratio of surface tension to centrifugal forces, and Re, the ratio of inertia to viscous forces.

The initial work on this topic was pioneered by Rayleigh (1879, 1892) who established stability criteria for stationary inviscid and viscous liquid columns in the absence of gravity. Interest in this subject has been revived in the last fifty years beginning with the work of Hocking & Michael (1959) who found that an inviscid liquid column uniformly spinning at angular rotation rate Ω is stable to planar disturbances of azimuthal mode number n provided

$$\gamma \geqslant \frac{\rho a^3 \Omega^2}{n(n+1)} \tag{1.1}$$

where γ is surface tension, ρ is fluid density, and a is the undisturbed column radius.

† Present address: US Bureau of Reclamation, Water Resources Research Laboratory, D-8560, P.O. Box 25007, Denver, CO 80225-0007, USA.

In a follow-on study to include the effect of viscosity, Hocking (1960) introduced the dimensionless parameter

$$L = \frac{\gamma}{\rho a^3 \Omega^2}, \tag{1.2}$$

an inverse rotational Bond number that Weidman, Goto & Fridberg (1997) have denoted the Hocking parameter. Hocking first showed that the criterion for stability of an inviscid liquid column, and a highly viscous one, subject to axisymmetric disturbances is given by

$$L \geqslant \frac{1}{k^2 - 1} \tag{1.3}$$

where k is the wavenumber normalized with column radius a. Hocking then hypothesized that this stability criterion for the viscous column would be independent of the rotational Reynolds number

$$Re = \frac{a^2 \Omega}{\nu} \tag{1.4}$$

in which ν is the kinematic viscosity of the fluid. Hocking next proved that the criterion for stability with respect to planar disturbances is the same in the limits of large and small Re, namely $L \geqslant 1/(n^2 - 1)$. Though unable to determine stability criteria at intermediate values of Re, he again argued that this criterion for planar disturbances would suffice for all Reynolds numbers.

Soon thereafter Gillis (1961) proved Hocking's conjecture, thereby confirming that the criterion for planar disturbances is independent of viscosity. Thus, the stability of planar disturbances for inviscid and viscous rotating liquid columns is given by the criteria

$$L \geqslant \frac{1}{n(n+1)} \qquad \text{(inviscid)}, \tag{1.5a}$$

$$L \geqslant \frac{1}{n^2 - 1} \qquad \text{(viscous)}. \tag{1.5b}$$

Since the $n = 1$ planar disturbance is neutrally stable, the region of stability is governed by $n = 2$ disturbances that for the inviscid case (1.5a) gives $L \geqslant 1/6$, while for the viscous case (1.5b) gives a smaller region of stability $L \geqslant 1/3$. Explanations concerning this non-intuitive result that viscosity decreases the range of stability have been given by Hocking (1960) and Yih (1960). Also, it is important to realize that in the region $1/6 \leqslant L \leqslant 1/3$ the invsicid $n = 2$ planar mode is neutrally stable.

Gillis & Kaufman (1962) subsequently considered the stability of a viscous rotating liquid column subject to three-dimensional disturbances. They were the first to ascertain the general stability criterion

$$L \geqslant \frac{1}{k^2 + n^2 - 1} \qquad \text{(viscous)} \tag{1.6}$$

which is again independent of the Reynolds number. In a note added in proof, they further showed that exchange of stability holds for axisymmetric disturbances. No determination of the most unstable modes outside the range of stability (1.6) was given.

Three decades later, Weidman (1994) reported general stability criteria for a rotating immiscible axisymmetric two-fluid system composed of an inner fluid core surrounded by an annular fluid layer bounded by a rigid cylinder. The entire system was assumed to be in uniform rotation, and both inviscid and viscous fluids were considered. The inviscid problem depends on the Hocking parameter L, the two-fluid density

ratio λ, and its radius ratio η while the viscous problem depends additionally on the Reynolds number *Re*. *Inter alia*, Weidman (1994) proved that exchange of stability for this two-fluid system holds for axisymmetric disturbances for both inviscid and viscous liquids.

In a follow-on study, Weidman *et al.* (1997, hereafter referred to as WGF) computed, for the inviscid two-fluid system described above, most unstable wavenumbers and frequencies for all preferred modes over a large range of L, λ and η parameter space. A subset of their results, the limiting case of a single rotating inviscid liquid column, provides the framework for analysis of the viscous problem considered here. Two key results from that inviscid investigation are pertinent to the present study. First, spiral modes never dominate, leaving axisymmetric modes preferred for $L > L_c$ and planar modes preferred for $L < L_c$, where $L_c = 0.1053$. Second, the transitions L_t between preferred n and $n+1$ planar modes are given by

$$L_t = \frac{1}{3n(n+1)} \qquad (n \geqslant 2) \qquad \text{(inviscid)}. \tag{1.7}$$

Stability studies on certain variants of the single- and two-fluid rotating columns have appeared in the literature. Gillis & Suh (1962) investigated the stability of a rotating system in which either a viscous or inviscid cylindrical column surrounds a solid core. Eggers & Brenner (1999) investigated the nonlinear pinch-off phenomenon in a uniformly spinning viscous liquid column. Dávalos-Orozco & Vázquez-Luis (2003) extended the two-fluid inviscid results of WGF to likewise include a solid core. Most recently, Ashmore & Stone (2004) considered the rotating immiscible two-fluid column in the large-viscosity and quasi-static limits for application to the spinning drop tensiometer.

From an experimental perspective, we find no published literature directly related to the determination of growth rates for the rotating liquid column. However, experimental investigations related to stationary liquid columns have been conducted. Most notably, Donnelly & Glaberson (1965) as well as Goedde & Yuen (1970) explored the capillary instability of viscous liquid jets and showed close agreement between measured growth rate curves and those predicted by the linear stability analyses of Rayleigh (1945) and Chandrasekhar (1961). The nonlinear breakup processes were studied by Rutland & Jameson (1970) for the purpose of droplet size prediction. Comparison of theoretical predictions with experimental observations in that case showed only partial agreement in that satellite droplets, not predicted by theory, were observed for dimensionless wavenumbers exceeding $k = 0.7$. The two experimental investigations by Donnelly & Glaberson (1965) and Goedde & Yuen (1970) suggest the possibility of exploring, via similar methods, the effect of viscosity on the stability of rotating liquid columns.

It would appear that the role of viscosity has been theoretically established for the rotating liquid column, i.e. its effect is simply to increase the range of unstable planar modes. However, with the exception of the Reynolds number variation of growth rates for viscous planar modes computed at three values of L plotted in Gillis (1961), we are not aware of any computations carried out to ascertain preferred modes of instability. The results presented in this study close the knowledge gap by identifying the most unstable modes, wavenumbers, and frequencies over the entire region of L–*Re* parameter space. A further goal is to pinpoint how viscosity modifies the surface-tension-driven instability of an inviscid rotating liquid column.

The presentation begins with the problem formulation for linearized temporal disturbances in § 2. Analytic solutions for the velocity and pressure fields lead

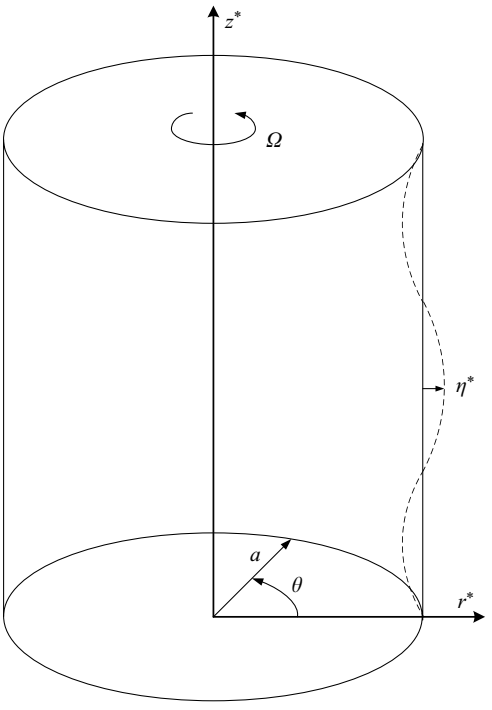

FIGURE 1. Section of an infinitely long liquid column with undisturbed radius a rotating at uniform angular velocity Ω showing the cylindrical coordinates and position of the disturbed free surface $r^* = a + \eta^*(\theta, z^*; t^*)$.

to a general viscous eigenvalue equation for three-dimensional disturbances. The associated limiting forms for the inviscid case, as well as the reduced forms for viscous axisymmetric ($n = 0$) and viscous planar ($k = 0$) disturbances are given in § 3. Numerical results demonstrating asymptotic consistency with previous work, and the effect of viscosity, are presented in § 4. A brief discussion of results and concluding remarks are given in § 5.

2. Problem formulation

A liquid column of density ρ and kinematic viscosity ν, rotating at uniform angular velocity Ω in the absence of gravity is depicted in figure 1. Relative to the rotating frame of reference, cylindrical polar coordinates $\boldsymbol{r}^* = (r^*, \theta, z^*)$ and coordinate velocities $\boldsymbol{u}^* = (u^*, v^*, w^*)$ are employed. Fluid motion in this rotating frame is governed by the incompressible continuity and Navier–Stokes equations

$$\nabla^* \cdot \boldsymbol{u}^* = 0, \tag{2.1a}$$

$$\frac{\mathrm{D}\boldsymbol{u}^*}{\mathrm{D}t^*} + 2(\boldsymbol{\Omega}^* \times \boldsymbol{u}^*) = -\frac{1}{\rho}\nabla^* p^* + \frac{1}{2}\nabla|\boldsymbol{u}^* \times \boldsymbol{r}^*|^2 + \nu\nabla^{*2}\boldsymbol{u}^*. \tag{2.1b}$$

Scaling lengths with a, velocities with $a\Omega$, time with Ω^{-1}, and pressure with $\rho a^2\Omega^2$, the component equations may be written

$$\frac{\partial u}{\partial r} + \frac{u}{r} + \frac{1}{r}\frac{\partial v}{\partial \theta} + \frac{\partial w}{\partial z} = 0, \tag{2.2a}$$

$$\frac{\partial u}{\partial t} + (\boldsymbol{u}\cdot\nabla)u - \frac{v^2}{r} - 2v = -\frac{\partial}{\partial r}\left(p - \frac{r^2}{2}\right) + \frac{1}{Re}\left(\nabla^2 u - \frac{u}{r^2} - \frac{2}{r^2}\frac{\partial v}{\partial \theta}\right), \tag{2.2b}$$

$$\frac{\partial v}{\partial t} + (\boldsymbol{u}\cdot\nabla)v + \frac{uv}{r} + 2u = -\frac{1}{r}\frac{\partial p}{\partial \theta} + \frac{1}{Re}\left(\nabla^2 v - \frac{v}{r^2} + \frac{2}{r^2}\frac{\partial u}{\partial \theta}\right), \tag{2.2c}$$

$$\frac{\partial w}{\partial t} + (\boldsymbol{u}\cdot\nabla)w = -\frac{\partial p}{\partial z} + \frac{1}{Re}\nabla^2 w, \tag{2.2d}$$

where $(r,\ \theta,\ z)$ are dimensionless polar coordinates; $(u,\ v,\ w)$ are dimensionless velocities in the direction of unit vectors $(\boldsymbol{e}_r, \boldsymbol{e}_\theta, \boldsymbol{e}_z)$, respectively; p is the dimensionless pressure; $Re = a^2\Omega/\nu$ is the rotational Reynolds number; and ∇ and ∇^2 are the cylindrical gradient and Laplacian operators

$$\nabla = \frac{\partial}{\partial r}\boldsymbol{e}_r + \frac{1}{r}\frac{\partial}{\partial \theta}\boldsymbol{e}_\theta + \frac{\partial}{\partial z}\boldsymbol{e}_z, \qquad \nabla^2 = \frac{1}{r}\frac{\partial}{\partial r}\left(r\frac{\partial}{\partial r}\right) + \frac{1}{r^2}\frac{\partial^2}{\partial \theta^2} + \frac{\partial^2}{\partial z^2}. \tag{2.3}$$

2.1. *Linearized disturbance equations*

The base state in the rotating frame of reference is one of zero velocity and undisturbed free surface located at $r^* = a$, in which case the dimensional governing equations (2.1*b*) reduce to a single equation for the radial pressure distribution

$$\frac{\mathrm{d}p^*}{\mathrm{d}r^*} = \rho\Omega^2 r^*. \tag{2.4}$$

Integrating, taking into account the capillary pressure jump $p^* = \gamma/a$ at $r^* = a$, where γ is the surface tension, gives, upon converting to dimensionless variables, the base-state pressure distribution

$$p(r) = L + \tfrac{1}{2}(r^2 - 1) \tag{2.5}$$

where $L = \gamma/\rho a^3\Omega^2$ is the Hocking parameter adopted to measure the effect of surface tension, which is the cause of instability in both rotating and non-rotating liquid columns.

Introducing arbitrary small disturbances to the base state, substituting into the governing equations, neglecting second-order terms, and eliminating the base-state solution gives the dimensionless linearized disturbance equations

$$\frac{\partial u}{\partial r} + \frac{u}{r} + \frac{1}{r}\frac{\partial v}{\partial \theta} + \frac{\partial w}{\partial z} = 0, \tag{2.6a}$$

$$\frac{\partial u}{\partial t} - 2v = -\frac{\partial p}{\partial r} + \frac{1}{Re}\left(\frac{\partial^2 u}{\partial r^2} + \frac{1}{r}\frac{\partial u}{\partial r} - \frac{u}{r^2} + \frac{1}{r^2}\frac{\partial^2 u}{\partial \theta^2} - \frac{2}{r^2}\frac{\partial v}{\partial \theta} + \frac{\partial^2 u}{\partial z^2}\right), \tag{2.6b}$$

$$\frac{\partial v}{\partial t} + 2u = -\frac{1}{r}\frac{\partial p}{\partial \theta} + \frac{1}{Re}\left(\frac{\partial^2 v}{\partial r^2} + \frac{1}{r}\frac{\partial v}{\partial r} - \frac{v}{r^2} + \frac{1}{r^2}\frac{\partial^2 v}{\partial \theta^2} - \frac{2}{r^2}\frac{\partial u}{\partial \theta} + \frac{\partial^2 v}{\partial z^2}\right), \tag{2.6c}$$

$$\frac{\partial w}{\partial t} = -\frac{\partial p}{\partial z} + \frac{1}{Re}\left(\frac{\partial^2 w}{\partial r^2} + \frac{1}{r}\frac{\partial w}{\partial r} + \frac{1}{r^2}\frac{\partial^2 w}{\partial \theta^2} + \frac{\partial^2 w}{\partial z^2}\right). \tag{2.6d}$$

These equations are to be solved with regularity and free surface conditions

$$u, v, w, p \quad \text{finite} \qquad (r = 0), \tag{2.7a}$$

$$u - \frac{\partial \eta}{\partial t} = 0 \qquad (r = 1), \tag{2.7b}$$

$$p + \left[\eta + L\left(\eta + \frac{\partial^2 \eta}{\partial \theta^2} + \frac{\partial^2 \eta}{\partial z^2}\right)\right] - \frac{2}{Re}\frac{\partial u}{\partial r} = 0 \qquad (r = 1), \tag{2.7c}$$

$$\frac{1}{r}\frac{\partial u}{\partial \theta} - \frac{v}{r} + \frac{\partial v}{\partial r} = 0 \qquad (r = 1), \tag{2.7d}$$

$$\frac{\partial u}{\partial z} + \frac{\partial w}{\partial r} = 0 \qquad (r = 1), \tag{2.7e}$$

where the position $r = 1 + \eta(\theta, z; t)$ of the disturbed free surface has been linearized to $r = 1$. Equation (2.7*b*) states that the free surface moves with the fluid, (2.7*c*) is continuity of normal stress at the free surface, and (2.7*d*, *e*) state that tangential stress components τ_{rz} and $\tau_{r\theta}$ vanish at the free surface.

2.2. *Temporal stability analysis*

The normal modes for disturbances that grow in time are posited as

$$\begin{pmatrix} \boldsymbol{u} \\ p \\ \eta \end{pmatrix} = \begin{bmatrix} \boldsymbol{U}(r) \\ P(r) \\ A \end{bmatrix} \mathrm{e}^{st + \mathrm{i}(n\theta + kz)} \tag{2.8}$$

where n is the azimuthal mode number, k is the dimensionless axial wavenumber, A is the disturbance amplitude, and $s = \sigma + \mathrm{i}\omega$ is the dimensionless complex growth rate in which σ is the real growth rate and ω is the frequency. All kinematics of the disturbances, including axial phase speed, rotational phase speed, and spiral inclination angle, may be calculated from the assumed modal form (2.8); see Appendix A of Ali (1988). Of interest for the presentation of results in §4 is the dimensionless phase speed C_θ at which planar and spiral disturbances rotate around the z-axis

$$C_\theta = -\frac{r\omega}{n}\Big|_{r=1} = -\frac{\omega}{n}, \tag{2.9}$$

relative to the rotating reference frame.

Substituting (2.8) into the linearized disturbance equations (2.6) yields

$$sU - 2V = -\frac{\mathrm{d}P}{\mathrm{d}r} + \frac{1}{Re}\left(\frac{\mathrm{d}^2U}{\mathrm{d}r^2} + \frac{1}{r}\frac{\mathrm{d}U}{\mathrm{d}r} - \frac{1}{r^2}U - \frac{n^2}{r^2}U - \frac{2\mathrm{i}n}{r^2}V - k^2U\right), \tag{2.10a}$$

$$sV - 2U = -\frac{\mathrm{i}n}{r}P + \frac{1}{Re}\left(\frac{\mathrm{d}^2V}{\mathrm{d}r^2} + \frac{1}{r}\frac{\mathrm{d}V}{\mathrm{d}r} - \frac{1}{r^2}V - \frac{n^2}{r^2}V + \frac{2\mathrm{i}n}{r^2}U - k^2V\right), \tag{2.10b}$$

$$sW = -\mathrm{i}kP + \frac{1}{Re}\left(\frac{\mathrm{d}^2W}{\mathrm{d}r^2} + \frac{1}{r}\frac{\mathrm{d}W}{\mathrm{d}r} - \frac{n^2}{r^2}W - k^2W\right), \tag{2.10c}$$

$$\frac{\mathrm{d}U}{\mathrm{d}r} + \frac{1}{r}U + \frac{\mathrm{i}n}{r}V + \mathrm{i}kW = 0, \tag{2.10d}$$

and corresponding boundary conditions (2.7) become

$$U, V, W, P \quad \text{finite} \qquad (r = 0), \tag{2.11a}$$

$$U - sA = 0 \qquad (r = 1), \tag{2.11b}$$

$$P + A[1 + L(1 - n^2 - k^2)] - \frac{2}{Re}\frac{\mathrm{d}U}{\mathrm{d}r} = 0 \qquad (r = 1), \tag{2.11c}$$

$$\mathrm{i}nU - V + \frac{\mathrm{d}V}{\mathrm{d}r} = 0 \qquad (r = 1), \tag{2.11d}$$

$$\mathrm{i}kU + \frac{\mathrm{d}W}{\mathrm{d}r} = 0 \qquad (r = 1). \tag{2.11e}$$

Note that viscosity appears via Re in both the disturbance equations (2.10*a–c*) and in the boundary condition (2.11*c*) for continuity of normal stress at the free surface.

2.3. *Solution of the disturbance equations*

The modal form of the linearized disturbance equations (2.10) may be rearranged to give

$$\frac{\mathrm{d}^2U}{\mathrm{d}r^2}+\frac{1}{r}\frac{\mathrm{d}U}{\mathrm{d}r}-\left(\frac{n^2+1}{r^2}+k^2+sRe\right)U=-Re\frac{\mathrm{d}P}{\mathrm{d}r}-\left(2Re-\frac{2\mathrm{i}n}{r^2}\right)V, \tag{2.12a}$$

$$\frac{\mathrm{d}^2V}{\mathrm{d}r^2}+\frac{1}{r}\frac{\mathrm{d}V}{\mathrm{d}r}-\left(\frac{n^2+1}{r^2}+k^2+sRe\right)V=\frac{\mathrm{i}n}{r}ReP+\left(2Re-\frac{2\mathrm{i}n}{r^2}\right)U, \tag{2.12b}$$

$$\frac{\mathrm{d}^2W}{\mathrm{d}r^2}+\frac{1}{r}\frac{\mathrm{d}W}{\mathrm{d}r}-\left(\frac{n^2}{r^2}+k^2+sRe\right)W=\mathrm{i}kReP, \tag{2.12c}$$

$$\frac{\mathrm{d}U}{\mathrm{d}r}+\frac{1}{r}U+\frac{\mathrm{i}n}{r}V+\mathrm{i}kW=0. \tag{2.12d}$$

The operator on the left-hand side of (2.12*c*) suggests that solutions for $W(r)$ and $P(r)$ may be found in terms of modified Bessel functions of order n. Insertion of $P(r)$ so determined into (2.12*a*) and (2.12*b*) then gives solutions for $U(r)$ and $V(r)$. In this manner one obtains disturbance velocity and pressure fields, regular on the axis of symmetry, given by

$$U(r)=\psi\left[(\alpha^2-k^2-sRe)I_n'(\alpha r)-2\mathrm{i}Re\frac{n}{\alpha r}I_n(\alpha r)\right], \tag{2.13a}$$

$$V(r)=-\mathrm{i}\psi\left[2\mathrm{i}ReI_n'(\alpha r)-(\alpha^2-k^2-sRe)\frac{n}{\alpha r}I_n(\alpha r)\right], \tag{2.13b}$$

$$W(r)=\mathrm{i}kI_n(\alpha r), \tag{2.13c}$$

$$P(r)=\left(\frac{\alpha^2-k^2-sRe}{Re}\right)I_n(\alpha r), \tag{2.13d}$$

where

$$\psi=\frac{\alpha(\alpha^2-k^2-sRe)}{[(\alpha^2-k^2)^2-2(\alpha^2-k^2)sRe+Re^2(s^2+4)]}. \tag{2.13e}$$

Finally, substitution of this velocity field into (2.12*d*) shows that the continuity equation is satisfied only for values of α satisfying

$$\alpha^6-(3k^2+2sRe)\alpha^4+(k^2+sRe)(3k^2+sRe)\alpha^2-k^2[(k^2+sRe)^2+4Re^2]=0. \tag{2.14}$$

At this point it appears that there are six independent solutions for the velocity and pressure fields. However, using the symmetry properties of modified Bessel functions, one can readily show that for n odd, U, V, W, P and all their higher derivatives are antisymmetric in α, while for n even they are all symmetric in α. Hence, there are only three independent solutions of the disturbance equations.

2.4. *The eigenvalue equation*

From (2.14) there exists three roots α_i^2 $(i=1, 2, 3)$. Owing to the above observation regarding solution symmetries, we associate the positive α_i roots with the three linearly independent solutions of U, V, W, P. The linear combination of the three solutions for each primitive variable constitutes their general solution. Evaluation of the free surface boundary conditions (2.11*b–e*) then gives rise to a set of three homogeneous

algebraic equations. A non-trivial solution of this system is obtained provided

$$\begin{vmatrix} P_1 + \dfrac{\beta}{s}U_1 - \dfrac{2}{Re}\dfrac{\mathrm{d}U_1}{\mathrm{d}r} & \mathrm{i}nU_1 - V_1 + \dfrac{\mathrm{d}V_1}{\mathrm{d}r} & \mathrm{i}kU_1 + \dfrac{\mathrm{d}W_1}{\mathrm{d}r} \\ P_2 + \dfrac{\beta}{s}U_2 - \dfrac{2}{Re}\dfrac{\mathrm{d}U_2}{\mathrm{d}r} & \mathrm{i}nU_2 - V_2 + \dfrac{\mathrm{d}V_2}{\mathrm{d}r} & \mathrm{i}kU_2 + \dfrac{\mathrm{d}W_2}{\mathrm{d}r} \\ P_3 + \dfrac{\beta}{s}U_3 - \dfrac{2}{Re}\dfrac{\mathrm{d}U_3}{\mathrm{d}r} & \mathrm{i}nU_3 - V_3 + \dfrac{\mathrm{d}V_3}{\mathrm{d}r} & \mathrm{i}kU_3 + \dfrac{\mathrm{d}W_3}{\mathrm{d}r} \end{vmatrix} = 0 \tag{2.15}$$

where U_i, V_i, W_i, their derivatives, and P_i, are all evaluated at $r = 1$ and $\beta = 1 + L(1 - n^2 - k^2)$. This is the same as the result obtained by Gillis & Kaufman (1962), but now written in the rotating reference frame using our dimensionless variables. They performed some numerical calculations and therefrom deduced the general stability criterion given by (1.6). The three roots α^2 of (2.14) are

$$\alpha_i^2 = \frac{1}{3}(3k^2 + 2sRe) - a_i \frac{s^2 Re^2}{6F(Re; s, k)} - b_i \frac{F(Re; s, k)}{6} \tag{2.16a}$$

where

$$a_1 = b_1 = -2, \qquad a_{2,3} = 1 \mp \mathrm{i}\sqrt{3}, \qquad b_{2,3} = 1 \pm \mathrm{i}\sqrt{3} \tag{2.16b}$$

and

$$F(Re; s, k) = Re^{2/3}(54k^2 - s^3 Re + 6k\sqrt{3(27k^2 - s^3 Re)})^{1/3}. \tag{2.16c}$$

Note that setting $k = 0$ in (2.14) gives the double root $\alpha^2 = sRe$ and the trivial root $\alpha^2 = 0$. The fact that these roots are not recovered as $k \to 0$ in (2.16) shows that this limit is non-uniform. We return to this point in § 3.3. Thus for $k \neq 0$, one may substitute (2.13) and (2.16) into (2.15) to obtain the eigenvalue equation and explore the stability of three-dimensional disturbances in L–Re parameter space.

3. Limiting cases

3.1. *Inviscid limit*

The general eigenvalue equation for the inviscid problem may be recovered directly from its viscous counterpart. Taking the limit $Re \to \infty$ of (2.14) and solving for α^2 yields

$$\alpha^2 = \frac{k^2}{s^2}(s^2 + 4). \tag{3.1}$$

Similarly, the limit as $Re \to \infty$ of (2.13) gives

$$U(r) = \frac{\alpha}{s^2 + 4}\left[s^2 I_n'(\alpha r) + \frac{2\mathrm{i}ns}{\alpha r} I_n(\alpha r)\right], \tag{3.2a}$$

$$V(r) = \frac{\mathrm{i}\alpha}{s^2 + 4}\left[2\mathrm{i}s I_n'(\alpha r) + \frac{ns^2}{\alpha r} I_n(\alpha r)\right], \tag{3.2b}$$

$$W(r) = \mathrm{i}k I_n(\alpha r), \tag{3.2c}$$

$$P(r) = -s I_n(\alpha r), \tag{3.2d}$$

and (2.11*b*,*c*) yield the combined kinematic–dynamic free surface condition

$$P + \frac{U}{s}[1 + L(1 - n^2 - k^2)] = 0 \qquad (r = 1). \tag{3.3}$$

Using (3.2), equation (3.3) may be evaluated at $r = 1$ to furnishe the inviscid eigenvalue equation

$$\alpha \frac{I_n'(\alpha)}{I_n(\alpha)} - \left[\frac{(s^2+4)}{1+L(1-n^2-k^2)} - \frac{2in}{s} \right] = 0, \tag{3.4}$$

in agreement with WGF.

3.2. *Viscous axisymmetric disturbances*

Setting $n = 0$ in (2.13) gives the reduced form of the velocity and pressure fields for axisymmetric disturbances

$$U(r) = \frac{\alpha(\alpha^2 - k^2 - sRe)^2}{[(\alpha^2-k^2)^2 - 2(\alpha^2-k^2)sRe + Re^2(s^2+4)]} I_0'(\alpha r), \tag{3.5a}$$

$$V(r) = \frac{2\alpha Re(\alpha^2 - k^2 - sRe)}{(\alpha^2-k^2)^2 - 2(\alpha^2-k^2)sRe + Re^2(s^2+4)} I_0'(\alpha r), \tag{3.5b}$$

$$W(r) = \mathrm{i}k I_0(\alpha r), \tag{3.5c}$$

$$P(r) = \frac{\alpha^2 - k^2 - sRe}{Re} I_0(\alpha r). \tag{3.5d}$$

Setting $n = 0$ in (2.15) gives the reduced eigenvalue equation for axisymmetric disturbances

$$\begin{vmatrix} P_1 + \dfrac{\beta}{s}U_1 - \dfrac{2}{Re}\dfrac{\mathrm{d}U_1}{\mathrm{d}r} & -V_1 + \dfrac{\mathrm{d}V_1}{\mathrm{d}r} & \mathrm{i}kU_1 + \dfrac{\mathrm{d}W_1}{\mathrm{d}r} \\ P_2 + \dfrac{\beta}{s}U_2 - \dfrac{2}{Re}\dfrac{\mathrm{d}U_2}{\mathrm{d}r} & -V_2 + \dfrac{\mathrm{d}V_2}{\mathrm{d}r} & \mathrm{i}kU_2 + \dfrac{\mathrm{d}W_2}{\mathrm{d}r} \\ P_3 + \dfrac{\beta}{s}U_3 - \dfrac{2}{Re}\dfrac{\mathrm{d}U_3}{\mathrm{d}r} & -V_3 + \dfrac{\mathrm{d}V_3}{\mathrm{d}r} & \mathrm{i}kU_3 + \dfrac{\mathrm{d}W_3}{\mathrm{d}r} \end{vmatrix} = 0 \tag{3.6}$$

where the velocities, pressures and appropriate derivatives are determined from (3.5), evaluated at $r = 1$. The three values of α^2 are still those given by (2.16), but now the axisymmetric form $\beta = 1 + L(1-k^2)$ is used in (3.6).

3.3. *Viscous planar disturbances*

Direct reduction to the planar eigenvalue equation cannot be obtained by setting $k = 0$ in (2.13) and (2.14) since the only non-trivial (double) root $\alpha^2 = sRe$ found from (2.14) gives $\psi = 0$ in (2.13*e*), which yields a trivial solution for the disturbance velocities in (2.13*a*, *b*). This is related to the zero-wavenumber non-uniformity discussed in § 2.4. Consequently, it is far easier to return to the modal form of the linearized disturbance equations (2.10) and boundary conditions (2.11), therein set $k = 0$, and solve the resulting equations. Following this procedure, one finds the disturbance velocity and pressure fields

$$U(r) = A\frac{in}{r} I_n(\alpha r) + Br^n, \tag{3.7a}$$

$$V(r) = -A\alpha I_n'(\alpha r) - Bnr^{n-1}, \tag{3.7b}$$

$$P(r) = -2AI_n(\alpha r) - B\mathrm{i}(s-2i)r^n, \tag{3.7c}$$

in which $\alpha^2 = sRe$ and $W(r)$ is set to zero without loss of generality. It is important to note that the regularity condition used to obtain solutions (3.7) requires $n \geqslant 0$ and hence no negative n solutions exist. Boundary constraints (2.11*b–e*) may be

consolidated into a combined kinematic–dynamic free surface condition and a single free stress condition, namely

$$P + \beta\frac{U}{s} - \frac{2}{Re}\frac{\mathrm{d}U}{\mathrm{d}r} = 0 \qquad (r = 1), \tag{3.8a}$$

$$\mathrm{i}nU - V + \frac{\mathrm{d}V}{\mathrm{d}r} = 0 \qquad (r = 1), \tag{3.8b}$$

where now the planar form $\beta = 1 + L(1 - n^2)$ is to be employed. Inserting (3.7) into (3.8) yields, after evaluation at $r = 1$, the viscous planar eigenvalue equation

$$\left[\alpha^2 + 2n - 2\alpha\frac{I_n'(\alpha)}{I_n(\alpha)}\right][\alpha^4 + 2(n^2 - 1)\alpha^2 - 2\mathrm{i}\alpha^2 Re - n\beta Re^2] - 2n(n-1)^2\alpha^4 = 0. \tag{3.9}$$

This reproduces the eigenvalue equation obtained by Hocking (1960) for viscous planar disturbances, after one replaces s by $s + \mathrm{i}n$ to transform from our rotating reference frame to his stationary frame of reference.

4. Results

A comprehensive understanding of the stability of the rotating liquid column requires an extensive numerical study of eigenvalue equation (2.15) for all n, k modes of instability over a large range of parameters L and Re. We begin with separate studies on the effect of viscosity for axisymmetric ($n = 0$) and planar ($k = 0$) disturbances and then lead into fully three-dimensional ($n \neq 0$ and $k \neq 0$) calculations. The most unstable modes are those exhibiting the largest growth rates for given parameter values. The underlying method of the numerical approach amounts to a root search stepping through parameter space to obtain the complex growth rates s for values of L, Re, n, and k. In the case of axisymmetric disturbances one can obtain growth rate curves for specified values of L and Re by stepping through values of k and solving the eigenvalue equation for the complex growth rate s. For planar disturbances the approach is the same except that there is a single growth rate for discrete values of n and each combination of L and Re. For three-dimensional disturbances one can specify combinations of L and Re, step through values of n, at each n step through values of k, and solve the eigenvalue equation for the complex growth rates. *Mathematica* (Wolfram 1999) was used for all computations reported here and the root search routine employed a modified secant method.

4.1. *Viscous axisymmetric disturbances*

Recalling that exchange of stability prevails for axisymmetric disturbances, one could *a priori* set $\omega = 0$. As a numerical check on this result, in the evaluation of eigenvalue equation (3.6) we have allowed for s to be complex. Indeed, solution values of ω were always numerically small, typically less than order 10^{-14}. Growth rate curves $\sigma = \sigma(k)$ were computed for order of magnitude variations of Re and L. To guide our study, we note that the general stability criterion given by (1.6) for $n = 0$ yields the cutoff wavenumber

$$k_{cut} = \sqrt{\frac{1}{L} + 1} \tag{4.1}$$

above which the viscous column is guaranteed to be stable, so the search is confined to wavenumbers $k < k_{cut}$. Many growth rate curves have been computed by Kubitschek (2006); here we exhibit two plots in figures 2(*a*) and 2(*b*) for $Re = 1.0$ and 1000,

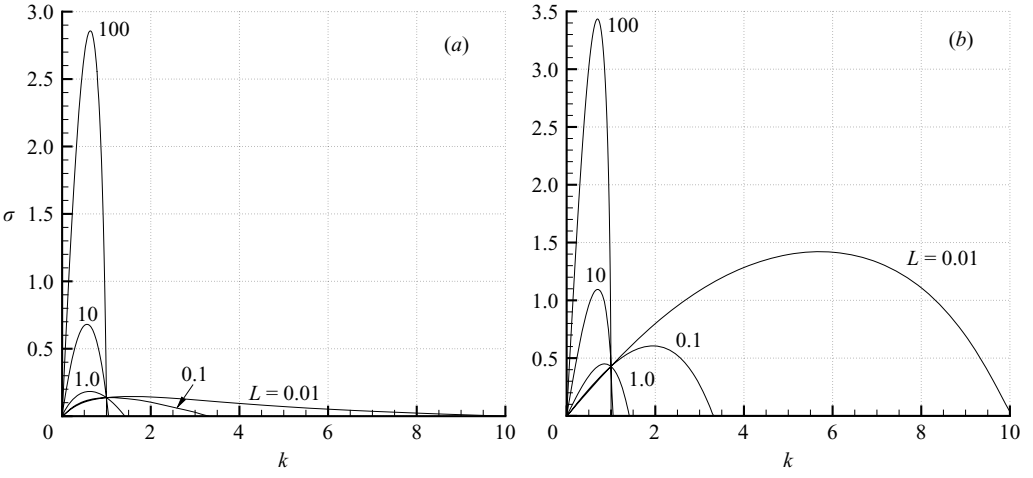

FIGURE 2. Wavenumber variation of growth rates for axisymmetric disturbances at selected values of L for (a) $Re = 1.0$ and (b) $Re = 1000$.

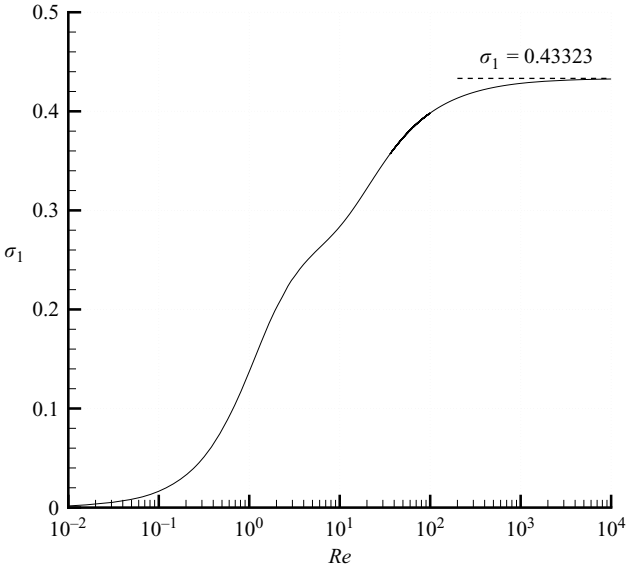

FIGURE 3. Reynolds number variation of growth rates for axisymmetric disturbances at $k = 1$ showing the approach as $Re \to \infty$ to the inviscid value $\sigma_1 = 0.43323$ reported in WGF.

respectively, with L varying in order of magnitude from 0.01 to 100. These results show that with L fixed, all growth rates increase with increasing Reynolds number, and the effect is most evident when L is small. It is also clear that at $k = 1$ the growth rates $\sigma_1 \equiv \sigma(k = 1)$ are independent of L, but vary with Re. We have computed the Reynolds number variation of σ_1 and show in figure 3 that it asymptotes smoothly to the value $\sigma_1 = 0.433228$ established by WGF for the inviscid liquid column. The L-variation of maximum growth rates σ_m, at selected values of Re, and their corresponding wavenumbers k_m, are displayed in figures 4(a) and 4(b). The lines connecting individual computed points aid in visualizing the trends. The results demonstrate that, at each

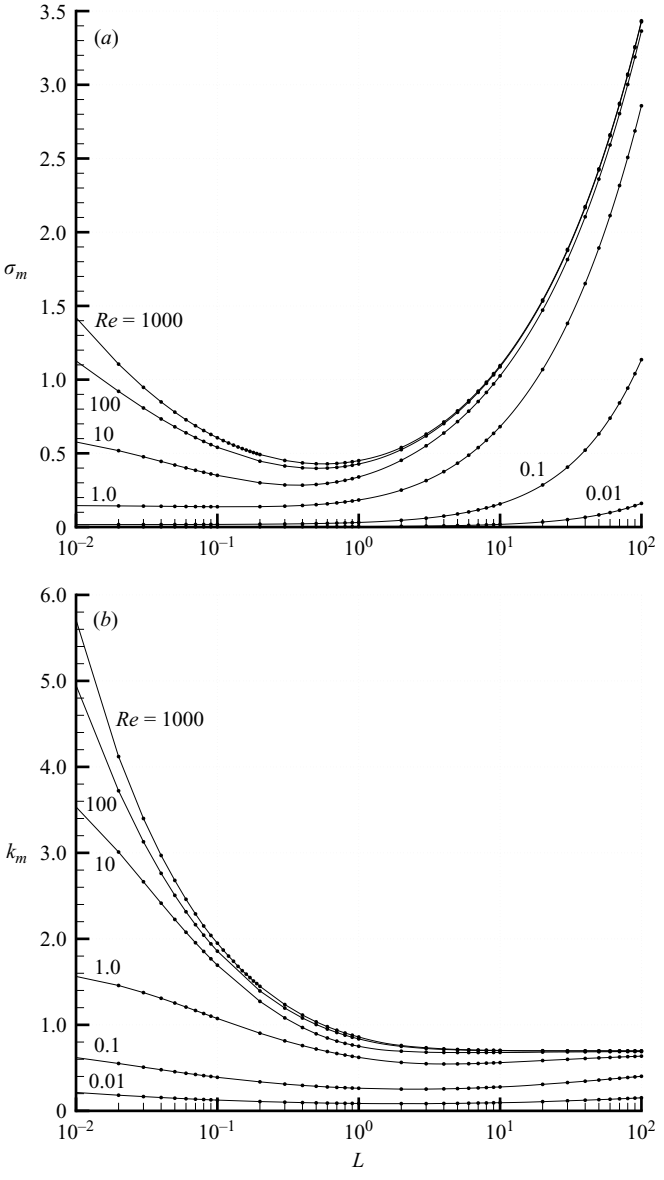

FIGURE 4. Summary of axisymmetric stability results showing the Hocking parameter variation of (*a*) maximum growth rates and (*b*) most unstable wavenumbers at selected values of *Re*.

value of L, increasing viscosity decreases the growth rates for axisymmetric disturbances and drives the most unstable wavenumber toward the long-wave limit $k = 0$.

Consistency of our computations for axisymmetric disturbances of a rotating column is provided by taking the $\Omega \to 0$ ($L \to \infty$) limit and comparing results with those obtained from Rayleigh's (1892) eigenvalue equation for a stationary liquid column given in the Appendix. This comparison requires a rescaling of σ_m that eliminates Ω. The connection between the maximum growth rates $\overline{\sigma}_m$ plotted in figure 15(*a*) and our maximum growth rates plotted in figure 4(*a*) is given by $\overline{\sigma}_m = \sigma_m / L^{1/2}$. The limiting behaviours of the (rescaled) maximum growth rates and

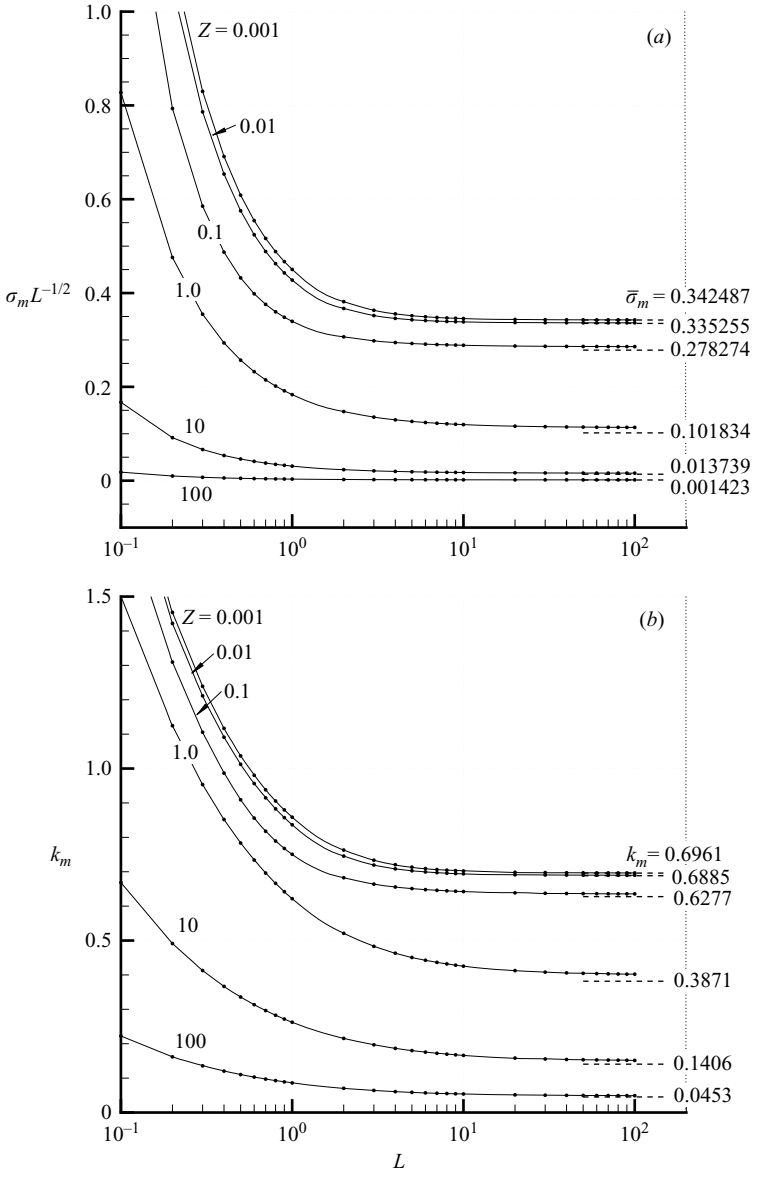

FIGURE 5. Hocking parameter variation of (*a*) rescaled maximum growth rates and (*b*) most unstable wavenumbers at selected values of the Ohnesorge number Z showing the stationary viscous column results given in figures 15(*a*, *b*).

most unstable wavenumbers at selected values of Ohnesorge number, defined as $Z = \mu/(\rho a \gamma)^{1/2}$, ranging in orders of magnitude from 0.001 to 100 are presented in figures 5(*a*) and 5(*b*), respectively. It is clear that, as $L \to \infty$, the maximum growth rates and corresponding wavenumbers for the rotating column approach the stationary column values shown by the dashed lines. Note the relatively fast convergence to Rayleigh's stationary liquid column results for Z small and large, compared to that for $O(1)$ values of Z.

4.2. *Viscous planar disturbances*

Equation (3.9) governs stability of the viscous rotating liquid column with respect to planar disturbances. Recall from § 3.3 that no planar modes exist for $n < 0$. Then, according to criterion (1.6), the search for unstable planar modes is necessarily limited to the segment $0 < L < 1/3$ for all Reynolds numbers. Figures 6(*a*) and 6(*b*) show the variation of planar growth rates σ and corresponding frequencies ω as a function of L for variations of Re ranging in orders of magnitude from 0.1 to 1000 obtained from solutions of (3.9). The stability boundaries shown at $L = 1/6$ and $L = 1/3$ in figures 6(*a*), 6(*b*) and 6(*c*) are predicted from (1.5*a*) and (1.5*b*) for the inviscid and viscous $n = 2$ cases, respectively. For L small, figure 6(*a*) shows that increasing Re brings about the appearance of successively higher preferred modes. Thus, the small-L behaviour for planar modes is in some sense analogous to that for axisymmetric disturbances (see figure 4*a*), namely that increasing the viscosity reduces the growth rate of the most unstable disturbance. Figure 6(*b*) displays the frequencies ω as a function of L at four values of Re ranging in orders of magnitude from 1 to 1000. At each Reynolds number, the largest frequency is attained by the lowest planar mode. Calculations show that $0 < \omega \leqslant 1.0$ in all cases where planar disturbances are found to be unstable. According to (2.9) the azimuthal phase speed of planar disturbances is $C_\theta = -\omega/n$. Since $\omega > 0$, we conclude that these disturbances are all retrograde, i.e. they travel in the direction opposite to that of column rotation viewed in the rotating frame of reference. Figure 6(*b*) also reveals that the $\omega = 1.0$ limit is being achieved for the $n = 2$ mode as $Re \to \infty$, consistent with the computations reported in WGF.

Of particular interest are the results in figure 6(*c*) that compare $n = 2$ planar mode growth rates for $Re = 1000$ with the inviscid results computed from the eigenvalue equation reported in Hocking & Michael (1959), transformed to our rotating reference frame. Only in the inviscid limit does the $n = 2$ planar growth rate become zero at $L = 1/6$, in which case that mode is neutrally stable in the region $1/6 \leqslant L \leqslant 1/3$. Thus our solution of the viscous eigenvalue equation confirms Hocking's (1960) observation that the effect of finite viscosity is to decrease the range of stability for planar disturbances from $L \geqslant 1/6$ to $L \geqslant 1/3$.

4.3. *Viscous three-dimensional disturbances*

4.3.1. *First spiral mode: $n = 1$*

The most general case for the viscous rotating liquid column is obtained when both $n \neq 0$ and $k \neq 0$. The regularity condition at $r = 0$ leading to disturbance solutions (2.13) establishes that it is sufficient to consider $n > 0$ only. In fact, the numerical results demonstrate a symmetry in solutions with respect to the sign of n. If for positive n one finds growth rates σ and frequencies ω, then negative n yields identical growth rates σ but with frequencies $-\omega$. Since the rotational speed of a spiral disturbance is given by (2.9), both positive and negative values of n give the same growth rates and identical retrograde motions.

The search for $n = 1$ unstable spiral modes is, according to stability criterion (1.6), confined to wavenumbers $k < k_{cut}$ where

$$k_{cut} = \sqrt{\frac{1}{L}} \qquad \text{(viscous)}. \tag{4.2}$$

Figures 7(*a*) and 7(*b*) show the wavenumber variation of growth rates and frequencies with Re at $L = 0.1$. This value of L has been chosen to effect a comparison with the inviscid results displayed in figures 4(*a*) and 4(*b*) of WGF where one finds that the unstable wavenumbers for $n = 1$ fall in the range $0.5 < k < k_{cut}$ and that the

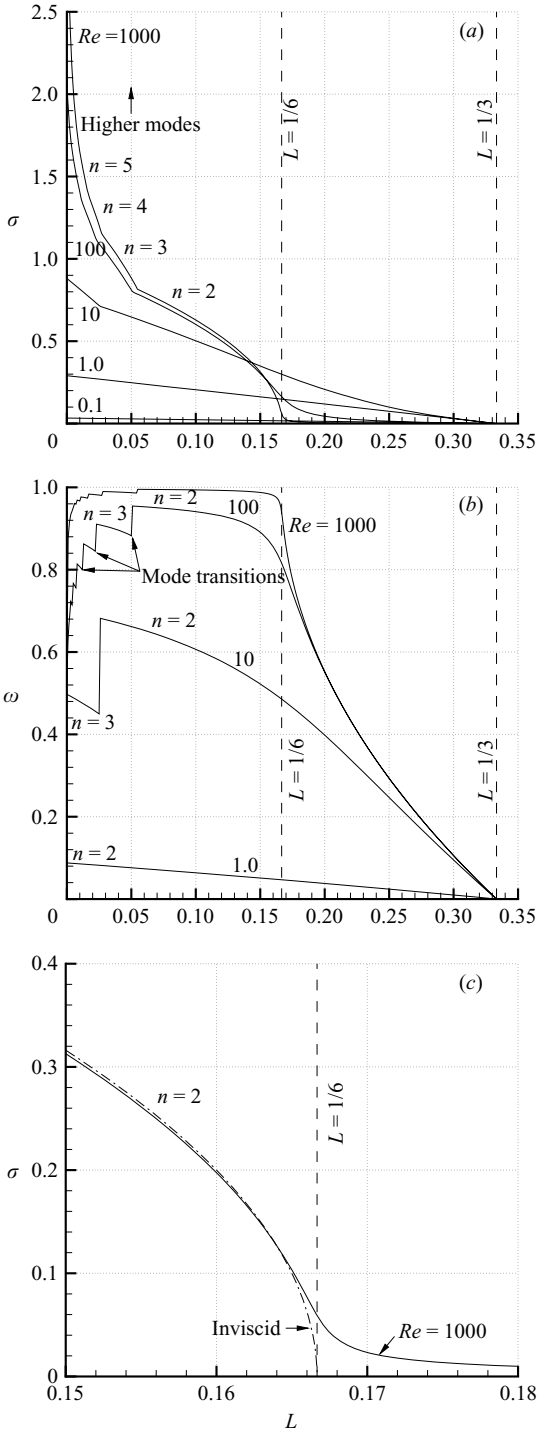

FIGURE 6. Hocking parameter variation of (*a*) preferred mode growth rates, (*b*) frequencies for viscous planar disturbances at selected values of *Re*, and (*c*) a comparison of the variation of the $n = 2$ viscous planar mode growth rate at $Re = 1000$ with the corresponding inviscid result in the neighbourhood of $L = 1/6$.

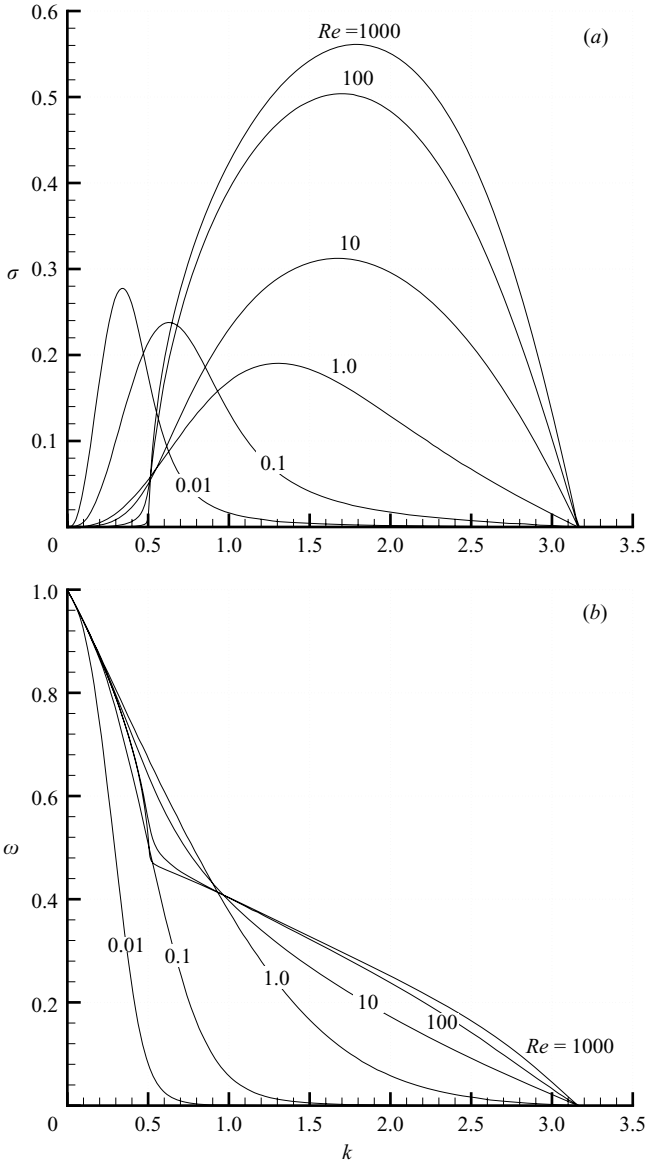

FIGURE 7. Wavenumber variation of $n=1$ spiral mode (a) growth rates and (b) frequencies for selected values of Re at $L=0.1$.

strip $0 \leqslant k \leqslant 0.5$ is rendered neutrally stable. The general rise in growth rates with decreasing Re in the segment $0 < k \leqslant 0.5$ shows that viscosity destabilizes the neutral inviscid spiral mode in this region. This phenomenon is akin to that found for planar modes where inviscid neutrally stable disturbances become unstable when viscosity is considered. Another key result is that $\sigma \to 0$ as $k \to 0$ for all Re, signifying that the $n=1$ viscous planar mode is always neutrally stable, as it is for the inviscid rotating liquid column.

Figures 8(a) and 8(b) show growth rates and frequencies at $L=10$. Here the region of neutral stability for inviscid disturbances (calculated from the inviscid eigenvalue equation for the $n=1$ spiral mode) has shrunk to $0 \leqslant k \leqslant 0.241$. The $\sigma(k)$ curve for

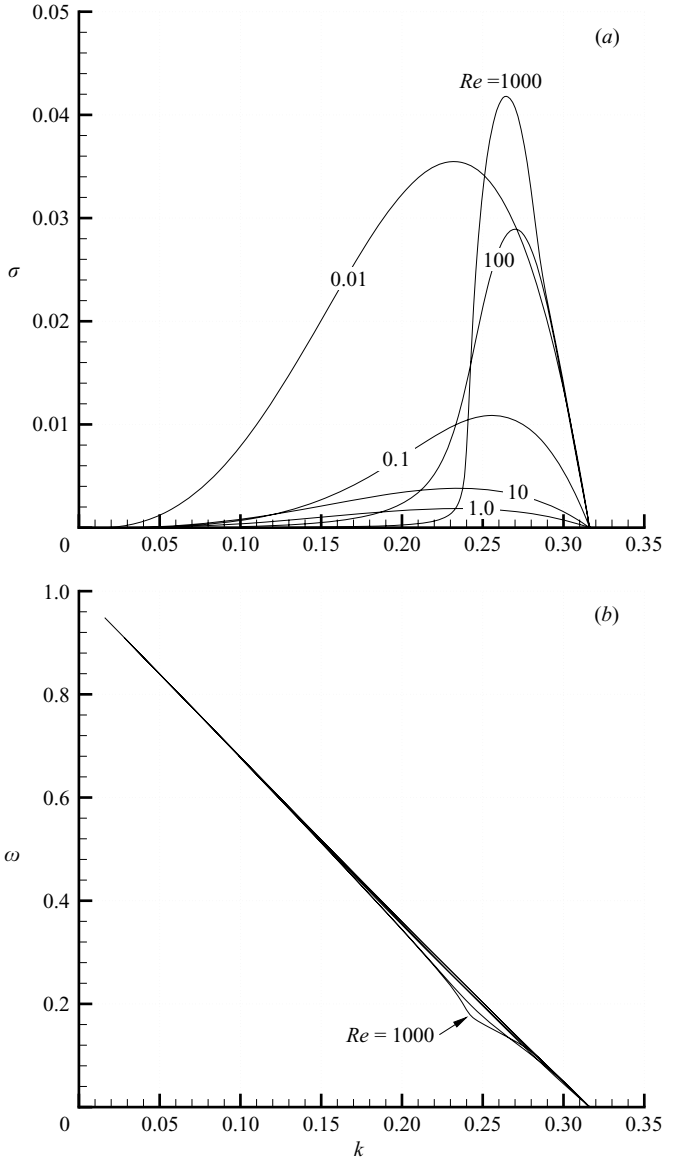

FIGURE 8. Wavenumber variation of $n = 1$ spiral mode (a) growth rates and (b) frequencies for selected values of Re at $L = 10$.

$Re = 1000$ in figure 8(a) shows the smooth approach with increasing Reynolds number to the $k = 0.241$ inviscid intercept. Note in figure 8(b) the evolution of the frequency distribution, at this elevated value of L, to a nearly Re-independent linear variation of ω with k.

The L variation of maximum growth rates σ_m, corresponding wavenumbers k_m, and frequencies ω_m for the $n = 1$ spiral disturbances are given in figures 9(a), 9(b) and 9(c) respectively for order of magnitude variations of Re spanning the range 0.01 to 1000. Similar to the planar and axisymmetric disturbances, at small L the growth rates increase monotonically with increasing Re; however, there exists an intermediate range $0.5 < L < 8.0$ where the growth rates at $Re = 0.01$ are most unstable. Motivated

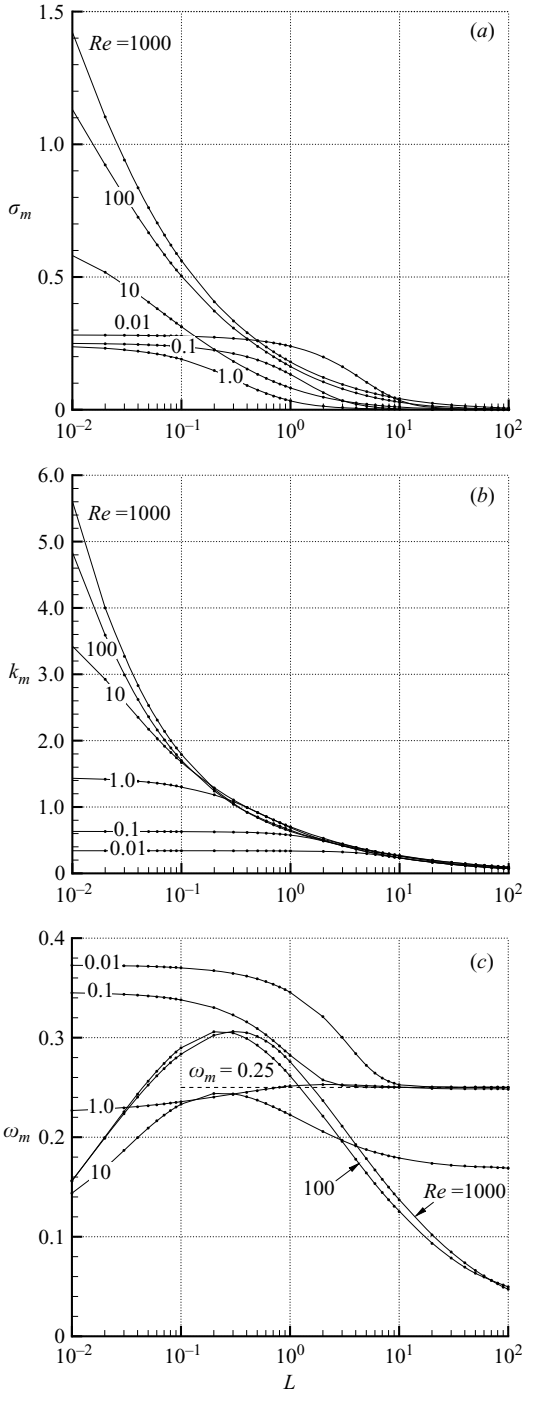

FIGURE 9. Summary of the $n = 1$ spiral mode results showing (*a*) maximum growth rates, (*b*) most unstable wavenumbers, and (*c*) frequencies as a function of L for selected values of Re.

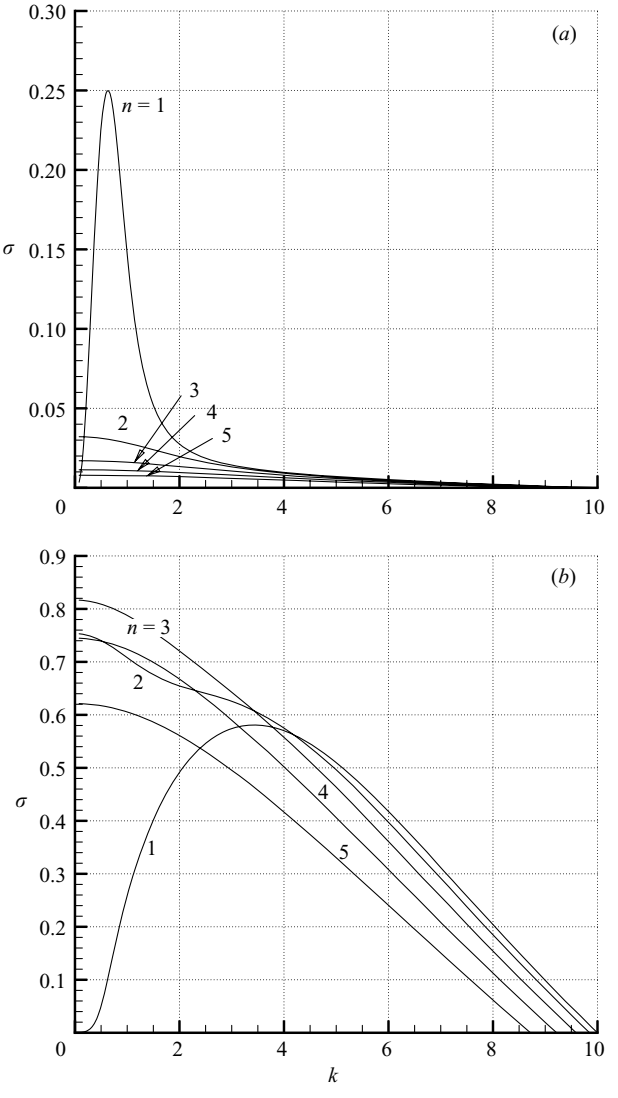

FIGURE 10. Wavenumber variation of growth rates for the first five spiral modes at $L = 0.01$ for (*a*) $Re = 0.1$ and (*b*) $Re = 10.0$.

by the small-Re behaviour of the disturbance frequency at large values of L seen in figure 9(*c*), we have endeavoured to compute the large-L, small-Re limit of ω_m. The result of this effort reveals, very accurately, the asymptotic limiting value $\omega_m = 1/4$. This feature is plotted as a horizontal dashed line in figure 9(*c*).

4.3.2. *Higher spiral modes: $n \geqslant 2$*

The stability of higher spiral modes was considered and growth rate curves were obtained for $n = 2, 3, 4, 5$. The results in figure 10 show two sets of spiral growth rate curves at $L = 0.01$, one at a small Reynolds number $Re = 0.1$ and the other at the larger value $Re = 10$. The small-Re results in figure 10(*a*) show that the lowest spiral mode is the most unstable uniformly in k. As Re increases, however, the higher modes compete with the fundamental mode. For example, the results in figure 10(*b*)

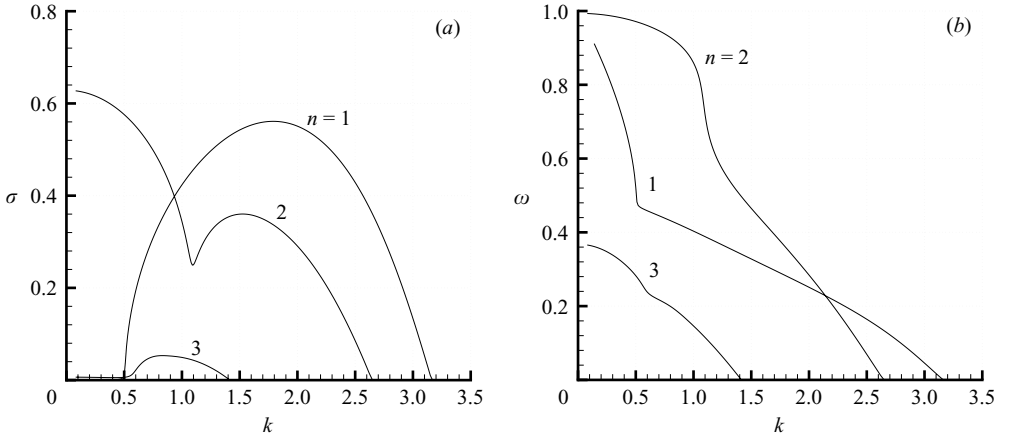

FIGURE 11. Wavenumber variation of (*a*) growth rates and (*b*) frequencies for the first three spiral modes at $L = 0.1$ and $Re = 1000$ demonstrating the smooth trend toward the inviscid results given in figures 4 and 5 of WGF.

at $Re = 10$ show that the $n = 1$ mode is most unstable in the range $4.18 < k < 10$, the $n = 2$ mode is most unstable in the range $3.42 < k < 4.18$, but it is the $n = 3$ mode that dominates in the $k \to 0$ (planar) limit. This is typical of all spiral modes $n \geqslant 2$, indicating that if their maximum growth rate surpasses that of the $n = 1$ mode, it does so at $k = 0$, i.e. they are planar modes. As a second example, we display growth rate and frequency curves for $n = 1, 2, 3$ at $L = 0.1$ and $Re = 1000$ in figure 11 computed for comparison with the corresponding $L = 0.1$ inviscid results given in figures 4 and 5 of WGF. The large-Re growth rate and frequency curves for the first three spiral modes further demonstrate that the transition to inviscid rotating column results is continuous and smooth.

4.4. *Mode competition*

Having determined the most unstable axisymmetric, planar, and spiral modes, we are now in position to determine which mode, at fixed values of L and Re, is preferred. The Hocking parameter variation of σ_m for the competing planar ($n \geqslant 2$), axisymmetric ($n = 0$) and spiral ($n = 1$) modes is plotted in figures 12(*a*), 12(*b*) and 12(*c*) for $Re = 10$, 1.0, 0.1, respectively. The results in figure 12(*a*) show that the column is dominated by planar and axisymmetric disturbances for all $L \geqslant 0.01$ (the smallest value investigated for non-zero k modes) with planar-to-axisymmetric mode transition at $(L_c)_1 = 0.1624$. At the smaller value $Re = 1.0$ in figure 12(*b*) the growth rate of the first spiral mode rises above the competing modes in the region $(L_c)_1 < L < (L_c)_2$ where $(L_c)_1 = 0.1371$ and $(L_c)_2 = 0.2251$. As the Reynolds number is decreased further to $Re = 0.1$ in figure 12(*c*), the $n = 2$ planar mode is no longer in contention, leaving the $n = 1$ spiral mode preferred up to $(L_c)_2 = 2.311$, above which the axisymmetric mode dominates. It is likely from the results in figures 12(*a*) and 12(*b*) that a tricritical point will appear when $(L_c)_1 = (L_c)_2$ somewhere in the range $1.0 < Re < 10$. An extensive search to find the tricritical point was performed by stepping through Re-space using a successive refinement approach and solving the eigenvalue equations for each mode to obtain their maximum growth rates as functions of L. The search was terminated when all maximum growth rates were found to be equivalent to within five digits at a single point (L_{tri}, Re_{tri}) in parameter space. This procedure yields the result plotted in figure 12(*d*) showing that $L_{tri} = 0.1807$ and $Re_{tri} = 1.1666$ (suspiciously close to 7/6) is

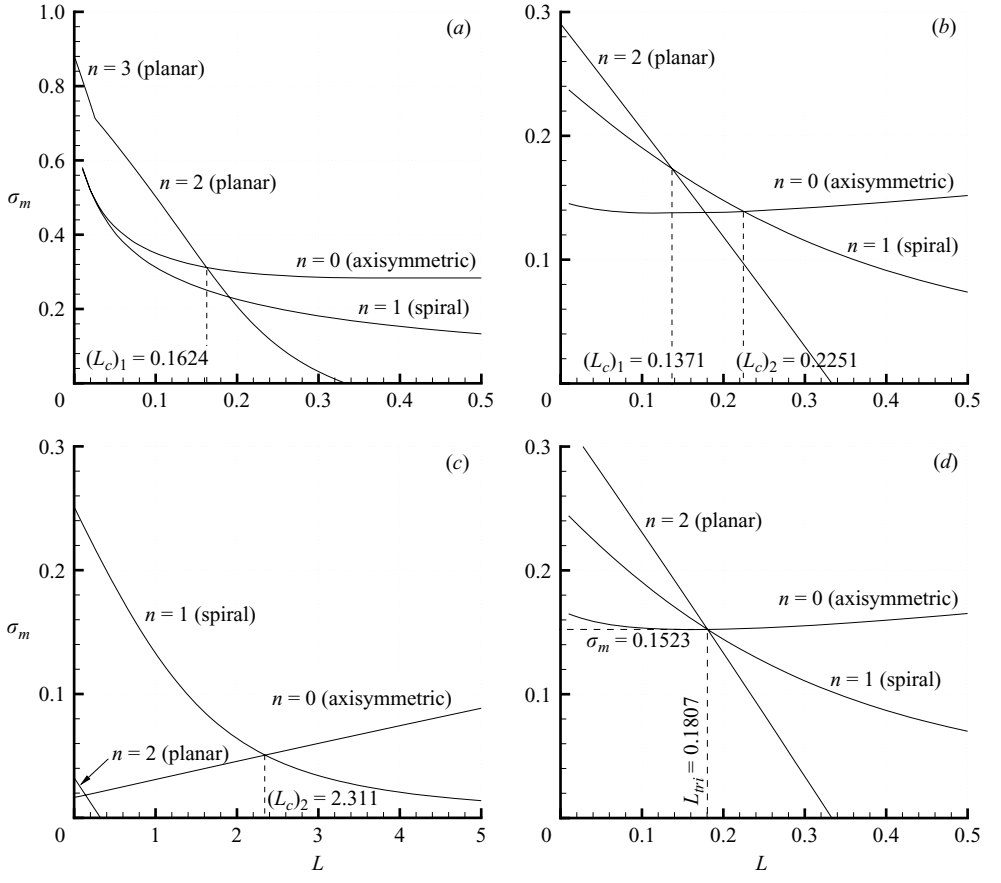

FIGURE 12. Hocking parameter variation of maximum growth rates for competing planar, axisymmetric, and $n=1$ spiral modes at (*a*) $Re=10.0$, (*b*) $Re=1.0$, (*c*) $Re=0.1$ and (*d*) $Re_{tri}=1.1666$. Numerical values for the planar–spiral crossovers $(L_c)_1$ and the spiral–axisymmetric crossovers $(L_c)_2$ are also indicated.

the point at which the maximum growth rates for the axisymmetric, $n=1$ spiral and $n=2$ planar modes attain the same value $\sigma_m=0.1523$. In the parlance of dynamical systems theory, the tricritical point is a co-dimension-two bifurcation. For Reynolds numbers larger than Re_{tri} only planar and axisymmetric modes are preferred, so this is the incipient Reynolds number below which the $n=1$ spiral mode appears. The existence of a spiral mode is a purely viscous result, since WGF have shown that there are no preferred spiral modes for the inviscid rotating liquid column.

It now should be clear that three distinct bifurcation curves emanate from the tricritical point to carve out three preferred mode regions in L–Re space. An algorithm was developed to compute these transition boundaries by accurately determining the intersection of maximum growth rate curves for competing modes. We denote T_{01} as the axisymmetric–spiral transition boundary, T_{02} as the axisymmetric–planar transition boundary, and T_{12} as the spiral–planar transition boundary. The results are displayed as figure 13 in which computed points have been connected by lines to aid in visualizing transition boundaries. This figure encapsulates all results of this study. For order of magnitude values of Re and L in each preferred mode region, one may find corresponding critical growth rates, wavenumbers and frequencies with

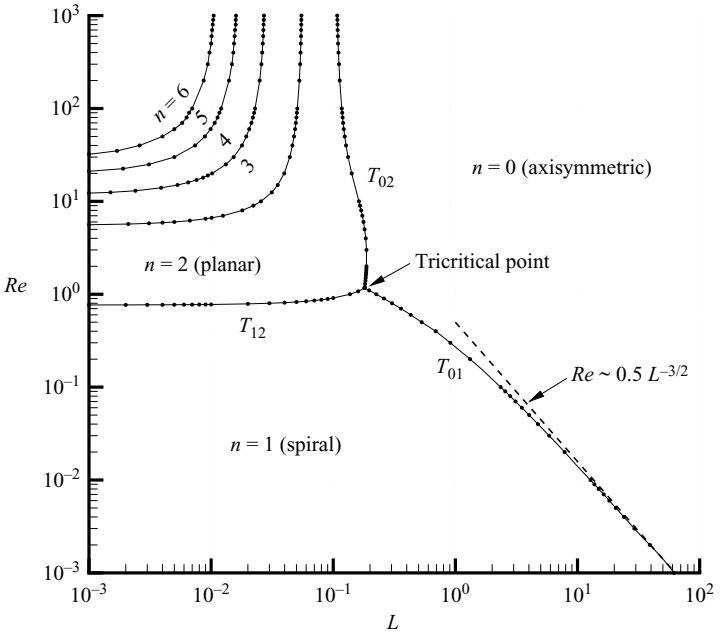

FIGURE 13. Preferred mode boundaries in L–Re space showing the planar, axisymmetric, and $n=1$ spiral mode regions and the tricritical point. Also shown as a dashed line is our estimate of the $L \to \infty$ asymptotic behaviour of the T_{01} transition boundary.

the aid of figure 4 for the axisymmetric mode, figure 6 for planar modes, and figure 9 for the $n=1$ spiral mode. From large-L and small-Re calculations of the T_{01} boundary, Kubitschek (2006) has found that the asymptotic behaviour is very closely $Re \sim 0.5L^{-3/2}$ ($L \to \infty$). Although this may be an exact asymptotic formula, we have not been able to determine the result analytically. This asymptote is plotted as the dashed line in figure 13.

An enlarged view of the region of preferred planar modes is presented in figure 14. The inviscid planar mode transitions L_t given by (1.7) are plotted as vertical dashed lines. Also plotted as a vertical dashed line is the transition $L_c = 0.1053$ separating inviscid axisymmetric modes from inviscid $n=2$ planar modes. As Re decreases, the nearly vertical viscous planar mode transition boundaries bend around to form horizontal transition boundaries. The asymptotic behaviour as $L \to 0$ of these mode transitions, here denoted as Re_t, are readily calculated by setting L equal to zero in the algorithms developed to compute relevant transition boundaries. In a similar manner, the transition between the $n=1$ spiral mode and the $n=2$ planar mode, here denoted Re_c, has been numerically determined. The horizontal dashed lines in figure 14 represent these transition behaviours as $L \to 0$. It is important to note that preferred higher planar modes ($n > 6$), not displayed in figures 13 and 14, appear in succession and become more frequent as L decreases and Re increases, simultaneously.

5. Discussion and conclusion

Numerical calculations have been performed to map out growth rates, wavenumbers and frequencies of the most unstable modes for a rotating viscous liquid column in L–Re parameter space, where L is the Hocking parameter measuring the effect of

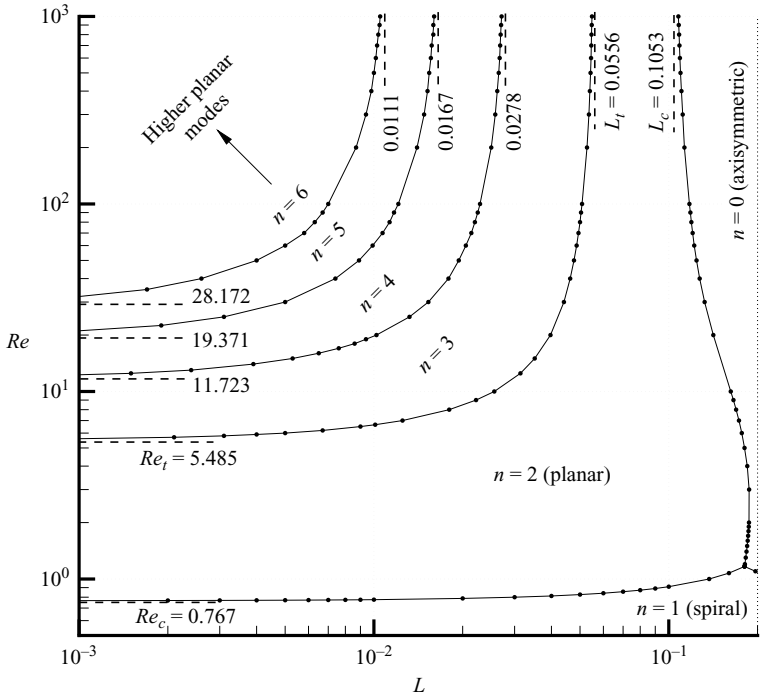

FIGURE 14. Preferred planar mode boundaries in L–Re space showing both the asymptotic $Re \to \infty$ (inviscid) transition boundaries L_t and L_c marked by vertical dashed lines and the asymptotic $L \to 0$ (viscous) transition boundaries Re_t and Re_c marked by horizontal dashed lines.

surface tension and Re is the rotational Reynolds number inversely measuring the effect of viscosity. The search of parameter space confirmed, and was guided by, the cutoff wavenumbers deduced from stability criterion (1.6) found by Gillis & Kaufman (1962). WGF have shown that only planar and axisymmetric modes are preferred in the inviscid limit, with axisymmetric modes appearing for $L > L_c$, where $L_c = 0.1053$, and planar modes appearing when $L < L_c$ with mode transitions given by (1.7). One effect of adding a small amount of viscosity to the rotating column is to eliminate the $n \to \infty$ planar modes. As the Reynolds number decreases, successively fewer planar modes are observed. Also, the planar–axisymmetric transition T_{02} varies little from its inviscid value L_c. Figure 14 shows that when $Re = 10$, only the second and third planar modes remain as $L \to 0$, though at $L = 0.01$ one can find six planar modes at sufficiently large values of Re. As the Reynolds number is reduced further to $Re_{tri} = 1.1666$, the appearance of an $n = 1$ spiral mode marks the end of the T_{02} boundary and the appearance of the planar–spiral T_{12} and axisymmetric–spiral T_{01} transition boundaries emanating from the tricritical point; see figure 13. At $Re = 0.767$ the T_{12} boundary disappears leaving only axisymmetric and first spiral modes as $Re \to 0$. The asymptotic behaviour of the T_{01} boundary separating these remaining preferred modes is very closely $Re \sim 0.5L^{-3/2}$ as $L \to \infty$.

The effect of viscosity is twofold. First, as noted by Hocking (1960), the region of stability of viscous planar modes is reduced to $L \geqslant 1/3$ from the region $L \geqslant 1/6$ for the inviscid case – viscosity destabilizes the inviscid neutral $n = 2$ planar mode in the region $1/6 < L < 1/3$. The fundamental spiral mode is similarly affected, i.e. $n = 1$

neutral mode segments of wavenumber space are destabilized by viscosity. Secondly, for wavenumbers away from these neutral mode segments, viscosity acts to stabilize the flow, in the sense that maximum growth rates decrease with decreasing Reynolds number. Likewise, viscosity reduces the maximum growth rates of axisymmetric modes uniformly in L.

The fundamental new result is the existence of a broad regime of preferred spiral instability in L–Re space. WGF have shown that for inviscid liquids, spiral modes are not preferred in either the single-fluid or the two-fluid rotating column. Although the $n=1$ mode first appears at a single (tricritical) point in parameter space, it is the only mode that persists as $Re \to 0$, uniformly in L, except in the limit of a stationary column in which case the mode of instability is axisymmetric in agreement with Rayleigh (1892).

As an interesting aside, we note that an $n=3$ retrograde spiral mode has been reported by Sanmiguel-Rojas & Fernandez-Feria (2006) for liquid flowing vertically down a tall narrow pipe discharging from a large concentric tank under the action of gravity. However, the mechanism of instability in that confined system is not surface tension, but instead the result of weak Coriolis forces that appear naturally at mid-latitude.

Extensions of the present work are numerous. Certainly a study of the three-dimensional instability of a two-fluid rotating viscous column with the approach taken here would be of interest. More interesting, especially in relation to experimental verification of our prediction of a tricritical point, would be to include the effect of a non-rotating gaseous ambient surrounding a rotating liquid column with uniform axial column translation. For this situation, the space of governing parameters would be significantly increased to include, at least, viscosity and density ratios and an axial Reynolds number. Moreover, the flow would become spatially dependent, warranting consideration of spatio–temporal stability.

Appendix. The stationary viscous column

For consistency, we seek to confirm that results computed from the full three-dimensional viscous rotating column coincide, in the proper limit, with the stationary viscous column results derived from Rayleigh's (1892) eigenvalue equation for axisymmetric disturbances. That equation is reproduced here in its original dimensional form

$$\begin{aligned}\frac{\gamma(1-k^2a^2)}{\rho a^3}\frac{ka}{n}\frac{k'^2-k^2}{k'^2+k^2}J_0'(\mathrm{i}ka)\\ =-2k^2\nu\left[J_0''(\mathrm{i}ka)-\frac{2kk'}{k'^2+k^2}\frac{J_0'(\mathrm{i}ka)}{J_0'(\mathrm{i}k'a)}J_0''(\mathrm{i}k'a)-\frac{k'(k'^2-k^2)}{k(k'^2+k^2)}\frac{J_0'(\mathrm{i}ka)}{J_0'(\mathrm{i}k'a)}J_0(\mathrm{i}k'a)\right]\\ +\frac{n}{ka}\left[\mathrm{i}ka\,J_0(\mathrm{i}ka)-\frac{2k^2}{k'^2+k^2}\frac{J_0'(\mathrm{i}ka)}{J_0'(\mathrm{i}k'a)}\mathrm{i}k'a\,J_0(\mathrm{i}k'a)\right],\end{aligned} \tag{A 1}$$

incorporating the J_0 Bessel function and its derivatives with complex arguments. Here k is the dimensional wavenumber, $k'^2=k^2+\mathrm{i}n/\nu$, and $\mathrm{i}n$ is the dimensional growth rate, our σ^*. Equation (A 1) may be written in dimensionless form in terms of a single parameter Z:

$$N_1+\bar{\sigma}ZN_2-\bar{\sigma}^2N_3=0, \tag{A 2a}$$

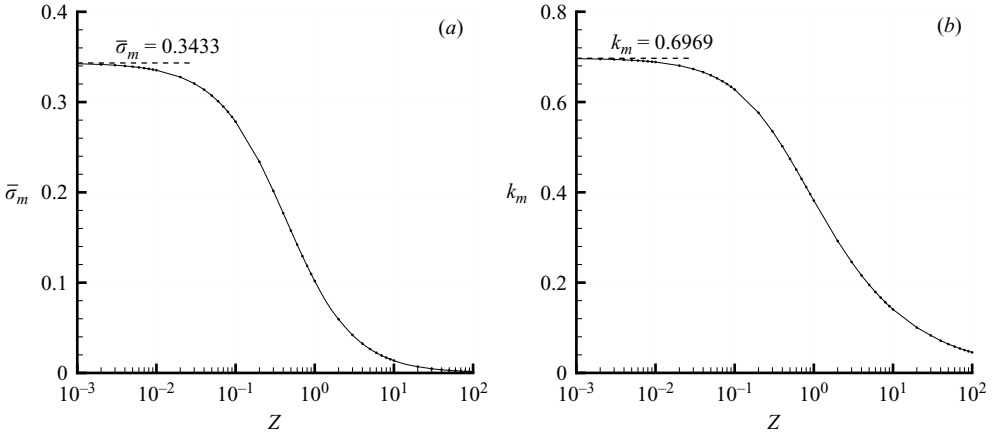

FIGURE 15. Stability results for a stationary viscous liquid column determined from Rayleigh's (1892) eigenvalue equation showing the Ohnesorge number variation of (*a*) maximum growth rates and (*b*) most unstable wavenumbers. The horizontal dashed lines give their $Z \to 0$ asymptotic behaviours.

where

$$N_1 = \mathrm{i}\kappa(1-\kappa^2)\frac{\kappa'^2-\kappa^2}{\kappa'^2+\kappa^2}J_0'(\mathrm{i}\kappa), \tag{A 2c}$$

$$N_2 = 2\kappa^2\left[J_0''(\mathrm{i}\kappa) - \frac{2\kappa\kappa'}{\kappa'^2+\kappa^2}\frac{J_0'(\mathrm{i}\kappa)}{J_0'(\mathrm{i}\kappa')}J_0''(\mathrm{i}\kappa') - \frac{\kappa'(\kappa'^2-\kappa^2)}{\kappa(\kappa'^2+\kappa^2)}\frac{J_0'(\mathrm{i}\kappa)}{J_0'(\mathrm{i}\kappa')}J_0(\mathrm{i}\kappa')\right], \tag{A 2b}$$

$$N_3 = J_0(\mathrm{i}\kappa) - \frac{2\kappa^2}{\kappa'^2+\kappa^2}\frac{\kappa'}{\kappa}\frac{J_0'(\mathrm{i}\kappa)}{J_0'(\mathrm{i}\kappa')}J_0(\mathrm{i}\kappa'), \tag{A 2d}$$

in which $\kappa = ka$ is the dimensionless wavenumber, $\kappa' = k'a$ such that $\kappa'^2 = \kappa^2 + \bar{\sigma}/Z$, and $\bar{\sigma} = \sigma^*(\rho a^3/\gamma)^{1/2}$. The single parameter governing axisymmetric stability of a stationary viscous column is the Ohnesorge number $Z = \mu/(\rho a\gamma)^{1/2}$ measuring the ratio of viscous to surface tension forces; its appearance in the eigenvalue relation is both explicit in (A 2*a*) and implicit through each appearance of κ'. Other than what can be interpolated from the nine listings in table LXII of Chandrasekhar (1961), there appears to be no published results of maximum growth rates and most unstable wavenumbers for the stationary viscous liquid column. Rayleigh (1892), however, did analyse (A 1) in the large-viscosity limit appropriate for liquid glass threads to show that "when viscosity is paramount long threads do not tend to divide themselves into drops at mutual distances comparable with the diameter of the cylinder, but rather to give way by attenuation at few and distant places".

We have solved Rayleigh's normalized eigenvalue equation (A 2) for the maximum growth rates $\bar{\sigma}_m$ and corresponding wavenumbers k_m as a function of Ohnesorge number Z. The maximum growth rates are plotted in figure 15(*a*), and the most unstable wavemumbers, denoted here as k_m ($\equiv\kappa_m$), are shown in figure 15(*b*). These results are used for comparison with the $\Omega \to 0$ limit of the rotating viscous liquid column in § 4.1.

REFERENCES

Ali, M. E. 1988 The stability of Taylor-Couette flow with radial heating. PhD thesis, University of Colorado, Boulder, CO.

Ashmore, J. & Stone, H. A. 2004 Instability of a rotating thread in a second immiscible liquid. *Phys. Fluids* **16**, 29–38.

Chandrasekhar, S. 1961 *Hydrodynamic and Hydromagnetic Stability*. Dover.

Dávalos-Orozco, L. A. & Vázquez-Luis, E. 2003 Instability of the interface between two inviscid fluids inside a rotating annulus in the absence of gravity. *Phys. Fluids* **15**, 2728–2739.

Donnelly, R. J. & Glaberson, W. 1965 Experiments on the capillary instability of a liquid jet. *Proc. R. Soc. Lond.* A **290**, 547–556.

Eggers, J. & Brenner, M. P. 1999 Spinning jets. *Proc. IUTAM Symp. on Nonlinear Waves in Multiphase Flow* (ed. H. C. Chang). Kluwer.

Gillis, J. 1961 Stability of a column of rotating viscous liquid. *Proc. Camb. Phil. Soc.* **57**, 152–159.

Gillis, J. & Kaufman, B. 1962 Stability of a rotating viscous jet. *Q. Appl. Maths* **19**, 301–308.

Gillis, J. & Suh, K. S. 1962 Stability of a rotating liquid column. *Phys. Fluids.* **5**, 149–155.

Goedde, E. F. & Yuen, M. C. 1970 Experiments on liquid jet instability. *J. Fluid Mech.* **40**, 495–511.

Hocking, L. M. 1960 The stability of a rigidly rotating column of liquid. *Mathematika* **7**, 1–9.

Hocking, L. M. & Michael, D. H. 1959 The stability of a column of rotating liquid. *Mathematika* **6**, 25–32.

Kubitschek, J. P. 2006 The effect of viscosity on the stability of a uniformly rotating viscous liquid column. PhD Thesis, University of Colorado, Boulder, CO.

Rayleigh, Lord 1879 On the stability of jets. *Proc. Lond. Math. Soc.* **9**, 4–13.

Rayleigh, Lord 1892 On the instability of a cylinder of viscous liquid under capillary force. *Phil. Mag.* **34**, 145–154.

Rayleigh, Lord 1945 *The Theory of Sound*, vol. II, 2nd edn. Dover.

Rutland, D. F. & Jameson, G. J. 1970 Theoretical prediction of the sizes of drops formed in the breakup of capillary jets. *Chem. Engng Sci.* **25**, 1689–1698.

Sanmiguel-Rojas, E. & Fernandez-Feria, R. 2006 Nonlinear instabilities in a vertical pipe flow discharging from a cylindrical container. *Phys. fluids* **18**, 024101.

Weidman, P. 1994 Stability criteria for two immiscible fluids rotating in zero gravity. *Mécanique Appliquée* **39**, 481–496.

Weidman, P. D., Goto, M. & Fridberg, A. 1997 On the stability of inviscid, rotating immiscible fluids in zero gravity. *Z. Agnew Math. Phys.* **48**, 921–950.

Wolfram, S. 1999 *Mathematica 4.0*. Wolfram Research, Inc.

Yih, C. S. 1960 Instability of a rotating liquid film with a free surface. *Proc. R. Soc. Lond.* A **258**, 63–89.